Water Ring Structure at DNA Interfaces: Hydration and Dynamics of DNA–Anthracycline Complexes[†,‡]

Leigh Ann Lipscomb, Mary Elizabeth Peek, Fang Xiao Zhou, Jay Aaron Bertrand, Donald VanDerveer, and Loren Dean Williams*

School of Chemistry & Biochemistry, Georgia Institute of Technology, Atlanta, Georgia 30332

Received October 22, 1993; Revised Manuscript Received January 27, 1994[⊗]

ABSTRACT: In crystallographic structures of biological macromolecules, one can observe many hydration rings that originate at one water molecule, pass via hydrogen bonds through several others, and return to the original water molecule. Five-membered water rings have been thought to occur with greater frequency than other ring sizes. We describe a quantitative assessment of relationships between water ring size and frequency of occurrence in the vicinity of nucleic acid interfaces. This report focuses on low-temperature X-ray crystallographic structures of two anthracyclines, adriamycin (ADRI) and daunomycin (DAUN), bound to d(CGATCG) and on several DNA structures published previously by others. We have obtained excellent low-temperature (−160 °C, LT) X-ray intensity data for d(CGATCG)–adriamycin and d(CGATCG)–daunomycin with a multiwire area detector. The LT X-ray data sets contain 20% (daunomycin, LT-DAUN) and 35% (adriamycin, LT-ADRI) more reflections than were used to derive the original room-temperature (15 °C) structures [Frederick, C. A., Williams, L. D., Ughetto, G., van der Marel, G. A., van Boom, J. H., Rich, A., & Wang, A. H.-J. (1990) *Biochemistry 29*, 2538–2549]. The results show that five-membered water rings are not preferred over other ring sizes. This assessment is consistent with our observation of broad dispersion W–W–W angles (σ = 20°). In addition, we report that the thermal mobility, distinct from the static disorder, of the amino sugar of daunomycin and adriamycin is significantly greater than that of the rest of the complex. This mobility implies that if the central AT base pair is switched to a CG base pair, there should be a low energy cost in avoiding the guanine amino group. The energy difference (for the sugar-binding preference) between d(CGTACG) and d(CGCGCG) could be considerably less than 20 kcal/mol, a value proposed previously from computation.

The importance of hydration in structure and conformation of DNA and DNA complexes is well recognized [see Berman (1991) for a recent review]. DNA conformation is strongly dependent on humidity. Near complete hydration, B-DNA prevails but converts to either A- or Z-conformation with reduced humidity. The 'spine of hydration' in the minor groove of crystal structures of B-DNA (Drew & Dickerson, 1981) has recently been observed in solution by NMR (Liepinsh et al., 1992).

In crystallographic structures of biological macromolecules, one can observe many hydration rings that originate at one water molecule, pass via hydrogen bonds through several others, and return to the original water molecule. In interfacial water, five-membered water rings are thought to occur with greater frequency than other ring sizes (n = 3, 4, 6, 7, where n = the number of water molecules in a ring). This five-membered ring motif originates from crystal structures of hydrated clathrates. In structures of hydrated clathrates, nonpolar molecules are enclosed by cages composed primarily of five-membered water rings (Jeffrey & McMullan, 1967; Jeffrey, 1969).

Five-membered water rings analogous to those observed in clathrate structures have been reported near the surfaces of proteins (Baker et al., 1985; Teeter, 1984; Teeter & Whitlow, 1987), DNA, and DNA–drug complexes (Neidle et al., 1980; Kennard et al., 1986; Berman, 1991; Bingman et al., 1992; Schneider et al., 1992). For example, a network of five-membered water rings was observed at the surface of a B-DNA drug complex [d(CpG)–proflavine; Neidle et al., 1980]. Similarly, a ribbon of five-membered water rings was observed in the major groove of an A-DNA octamer [d(GG^{Br}UA^{Br}UACC); Kennard et al., 1986].

This report describes a quantitative assessment of relationships between water ring size and frequency of occurrence in the vicinity of nucleic acid interfaces. Our original intention was to measure populations of ring types to determine their relative free energies of formation. Surprisingly, we have found no evidence that five-membered water rings are preferred over other ring sizes. Further, in a search for physical basis for the preference for five-membered water rings, we have examined the distribution of hydrogen-bond angles and lengths. The most reasonable explanation for preference for five-membered water rings would be the correspondence between the angles within a planar pentagon (108°) and those within a tetrahedron, the preferred arrangement of water molecules. However, in the absence of a constraint to planarity, it is possible to construct a variety of ring sizes with appropriate angles. Further, we observe that although water–water–water angles average 105°, close to the value expected within planar pentagons, the dispersion of angles (σ = 20°) is broad. This dispersion, coupled with a lack of any general constraint to planarity, implies that pentagons might not occur with greater frequency than other ring types.

This report focuses on low-temperature crystal structures of two anthracyclines, adriamycin (ADRI) and daunomycin

[†] This work was funded by the American Cancer Society (NP-831).

[‡] The atomic coordinates have been deposited with the Brookhaven Protein Data Bank under file names 151D (LT-ADRI) and 152D (LT-DAUN).

* Author to whom correspondence should be addressed.

[⊗] Abstract published in *Advance ACS Abstracts*, March 1, 1994.

0006-2960/94/0433-3649$04.50/0

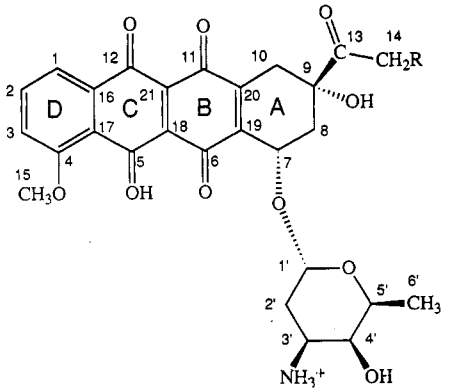

FIGURE 1: Chemical structures of anthracyclines. In daunomycin, R = H, and in adriamycin, R = OH.

(DAUN), bound to DNA, and on several DNA structures published previously by others. ADRI and DAUN (Figure 1) are important cancer chemotherapeutic agents that intercalate in DNA and interfere with processes of replication and transcription (Acramone & Penco, 1989). While both drugs are active against Hodgkin's disease, lymphosarcoma, reticular sarcoma, and leukemia in children, adriamycin is more effective than daunomycin against solid tumors. Trail and co-workers (Trail et al., 1993) have recently demonstrated that immunoconjugates of daunomycin can induce complete regressions of human breast, lung, and colon carcinomas that are subcutaneously implanted in mice. In a recent estimation of the electrostatic contributions ($\Delta G_{el}°$) to the free energy of DNA–anthracycline binding, identical values of $\Delta G_{el}°$ for ADRI and DAUN were reported (Chaires et al., 1993). The large, negative values of $\Delta G°$ observed in that study are compatible with stabilization of DNA–anthracycline complexes largely by hydrogen bonding and van der Waal's interactions.

Such interactions have been observed in a series of high-resolution X-ray crystal structures of DNA–anthracycline complexes. In each X-ray structure, the intercalated chromophore stacks between adjacent base pairs and hydrogen bonds anchor the drug to the DNA. For the chromophore, certain direct (9-hydroxyl to guanine N2 and N3) and solvent-mediated (O4 and O5 to purine N7) hydrogen bonds have been observed in all DNA–anthracycline crystal structures reported thus far: d(CGTACG)–DAUN (Quigley et al., 1980; Wang et al., 1987), d(CGATCG)–ADRI (Frederick et al., 1990), d(CGATCG)–DAUN (Frederick et al., 1990; Moore et al., 1989), d(CGATCG)–4′-*epi*ADRI (Williams et al., 1990b), d(TGTACA)–DAUN (Nunn et al., 1991), d(TGATCA)–DAUN (Nunn et al., 1991), d(TGTACA)–4′-*epi*ADRI (Leonard et al., 1992), d(CGTsACG)–11-deoxyDAUN (Williams et al., 1990a), d(CGATCG)–4-*O*-demethyl-11-deoxyADRI (Gao & Wang, 1991), and d(CGATCG)–4-demethoxyDAUN (Gao & Wang, 1991). In contrast, considerable variation in the position of the drug amino sugar is observed. This led to the suggestion (Williams et al., 1990a) that the amino sugar experiences considerable mobility in solution. In d(CGTACG)–DAUN, d(TGTACA)–DAUN, and d(TGTACA)–4′-*epi*ADRI, the amino sugar does not form direct hydrogen bonds with the minor groove. However, if the sequence of the central base pairs is reversed [as in d(CGATCG)–ADRI, d(CGATCG)–DAUN, and d(TGATCA)–DAUN], the amino sugar drops within direct hydrogen-bonding distance of the minor-groove DNA atoms. When all DNA–anthracycline crystal structures are surveyed, the position of the amino sugar appears variable and difficult to rationalize. Here, we report that the thermal mobility of the amino sugar is greater than that of the rest of the complex.

EXPERIMENTAL PROCEDURES

Crystal Growth and Shock Cooling. The ammonium salt of reverse-phase-HPLC-purified d(CGATCG) was purchased from the Midland Certified Reagent Company (Midland, TX). Adriamycin and daunomycin (Sigma Chemical Company, St. Louis, MO) were used without purification. Crystals were grown from sitting drops that initially contained 0.9 mM d(CGATCG), 40 mM sodium cacodylate (pH = 6.5), 4.2 mM $MgCl_2$, 5% 2-methyl-2,4-pentanediol (MPD), 8.3 mM spermine hydrochloride, and 1.9 mM anthracycline. The drops were equilibrated by vapor diffusion against a reservoir containing 30% MPD. Tetragonal ($P4_12_12$) crystals appeared within 3 days (adriamycin) or 6 days (daunomycin) and grew to sizes of 0.46 mm × 0.34 mm (adriamycin, after 14 days) or 0.35 mm × 0.27 mm (daunomycin, after 27 days). A quartz fiber was mounted on a goniometer head, and the tip was coated with a small amount of silicone grease. The fiber was then placed directly into the sitting drop and touched to the crystal. Surface tension held the crystal on the fiber during shock cooling by submersion in liquid nitrogen. The crystal was quickly transferred from the liquid nitrogen to a goniostat that was bathed in a −160 °C (LT) stream of nitrogen vapor. Unit cell determinations indicated shrinkage in all dimensions relative to the RT (room-temperature) structure (see Table 1). In particular, the *c* axis was observed to shrink on shock cooling so that the average base pair/anthracycline stacking distance decreased from 3.32 Å (RT) to 3.27 Å (LT).

Data Collection and Refinement. X-ray intensity data were collected at −160 °C with a San Diego Multiwire Systems (SDMS) area detector (Xuong et al., 1985) and an Enraf-Nonius cryostat (Model FR558SH). Cu Kα radiation (1.54 Å) was generated with a fine-focus Rigaku RU200 rotating anode, and data were collected in the ω scan mode. The low-resolution data (>2.5 Å) were collected in two sweeps. The first sweep was collected at full generator power (100 mA, 46 kV). The frames containing extremely intense reflections (around 3.3 Å) were excluded from the data reduction process. To obtain accurate intensities of the intense reflections, a second low-resolution sweep was collected at reduced power (60 mA, 46 kV).

Excluding solvent molecules, the RT-d(CGATCG)–ADRI and RT-d(CGATCG)–DAUN coordinates (Frederick et al., 1990) were used as starting models for the refinements. The structures were refined, as were the RT structures, with Konnert–Hendrickson constrained least-squares methods (Hendrickson & Konnert, 1981) as modified for nucleic acids (Quigley et al., 1978). Sum ($2F_o - F_c$) and difference ($F_o - F_c$) Fourier maps were calculated with XPLOR (Brunger et al., 1987) and displayed on a Silicon Graphics 4D70GT graphics workstation. Manual manipulation of the models was performed with the program CHAIN (Sack, 1990). Solvent molecules were located from sum and difference maps and added in groups of 10 or less. Overlapping sum and difference density was the only requirement for addition of solvent molecules. Refinement statistics are presented in Table 1.

Data Quality. Collection of X-ray intensity data with an area detector is somewhat problematic with DNA crystals. The internal order of DNA (base stacking) causes a large dynamic range in the intensities of the X-ray reflections. Accurate intensities of large DNA stacking reflections (at around 3.3-Å resolution) cannot be measured simultaneously

Table 1: Room Temperature versus Cryo Crystallography for d(CGATCG)–Anthracycline Complexes

parameter	LT-DAUN	RT-DAUN	LT-ADRI	RT-ADRI
	Crystallographic Parameters			
cell constants (Å)	27.85	28.11	27.92	28.21
	27.85	28.11	27.92	28.21
	52.33	53.08	52.39	53.19
space group	$P4_12_12$	$P4_12_12$	$P4_12_12$	$P4_12_12$
	Data Collection and Refinement Statistics			
temperature (°C)	−160	15	−160	15
total no. of collected reflections	54233	N/A[a]	17251	N/A[a]
total no. of unique reflections	3817	3020	3402	2225
R merge (%)	8.54	N/A[a]	5.70	N/A[a]
R factor (%)	22.6	18.6	20.0	21.4
average $F_o - F_c$ discrepancy (%)	35.45	26.27	32.04	41.47
rms deviation of single bonds from ideality (Å)	0.027	0.039	0.024	0.028
rms deviation of planes from ideality (Å)	0.025	0.028	0.019	0.021
overdeterminacy ratio	4.5	3.6	3.8	2.6
no. of observed solvent molecules	55 H_2O	53 H_2O	62 H_2O	53 H_2O
		1 spermine		1 spermine
		1 sodium		1 sodium
	Breakdown of the No. of Reflections by Resolution Range			
minimum resolution (Å)				
5.00	89	111	37	113
3.00	367	397	362	399
2.50	314	333	333	313
2.00	690	706	718	585
1.70	882	785	862	512
1.50	990	663	729	268
1.20	485	25	361	35
	Breakdown of R Factor by Resolution Range R Factor (%)			
5.00	25.5	16.7	17.7	18.0
3.00	18.5	10.9	16.8	12.1
2.50	21.2	19.2	17.0	20.2
2.00	21.2	20.6	19.7	22.9
1.70	23.7	24.1	22.2	31.3
1.50	27.0	27.0	23.1	38.1
1.20	27.1	42.3[b]	26.5	56.4[b]

[a] N/A indicates that this information is not available. [b] The model was not refined against these data.

with those of the weakest reflections. Improper measurement of intense reflections will introduce errors during scaling. As described above, intense reflections were obtained at lower power than weaker reflections.

One initial goal of this work was to assess the quality of the data that could be obtained from nucleic acids at LT (−160 °C) with an area detector. A comparison of the RT (diffractometer) and LT (area detector) data collection and refinement statistics is presented in Table 1. The LT data sets contain 20% (daunomycin) and 35% (adriamycin) more unique reflections [$F > 1\sigma(F)$] than were used to derive the original RT structures (Frederick et al., 1990). The improvement in the LT data is most striking at high resolution between 1.7 and 1.2 Å, where the LT-DAUN and LT-ADRI data sets contain 38% and 58% more unique reflections than their RT counterparts. At low resolution between 5.0 and 10.0 Å, the RT data sets are 20% (daunomycin) and 67% (adriamycin) more complete. These percentages are misleading due to the small number of reflections with resolution lower than 5.0 Å. Actually, the 20% superiority of the RT daunomycin data set in this resolution range corresponds to only 22 additional reflections, while the 67% superiority of RT adriamycin data set corresponds to only 76 reflections. This contrasts with the high-resolution range between 1.7 and 1.2 Å, where the LT improvements of 38% (884 reflections, DAUN) and 58% (1137 reflections, ADRI) are much more significant. Observation of a greater number of reflections led to improved overdeterminacy ratios (see Table 1). The R factor of 22.6% for LT-DAUN is higher than that of RT-DAUN (18.6%); however, the LT maps are significantly sharper and more detailed. It is possible that a slight increase in the crystal mosaicity upon shock cooling ultimately resulted in a higher R factor.

Cyclic Structures. A computer program entitled CYCLONE was designed to count numbers of n-membered water rings present in a specified volume. CYCLONE initially sets up a matrix of all interatomic contacts and then sorts the matrix to count rings. CYCLONE was carefully tested on coordinate files containing known numbers of three-, four-, five-, six-, and seven-membered rings. CYCLONE was used to count n-membered rings near LT-ADRI, d(CpG)–proflavine, and d(GG^{Br}UA^{Br}UACC). The coordinates of d(CpG)–proflavine were obtained from the Nucleic Acid Database (Berman et al., 1992), while the d(GG^{Br}UA^{Br}UACC) coordinates were graciously provided by Dr. Olga Kennard (Cambridge). MINITAB (Statistical Software by Minitab Inc., State College, PA) was used to calculate linear least-squares fits and 95% confidence regions.

Edge effects do not significantly alter the relative frequencies of the various ring types. The potential for this type of error arises because water molecules near the edge of the box form cyclic structures uncounted by CYCLONE. To test for the significance of edge effects in the results obtained with CYCLONE, the numbers of n-membered rings around a single DNA duplex were compared to those obtained when employing a much larger box, i.e., when three adjacent duplexes plus surrounding water molecules were used. This triples the volume of the box considered by CYCLONE, decreasing edge effects by increasing the ratio of volume to surface area. Symmetry operators were used to generate duplexes two and

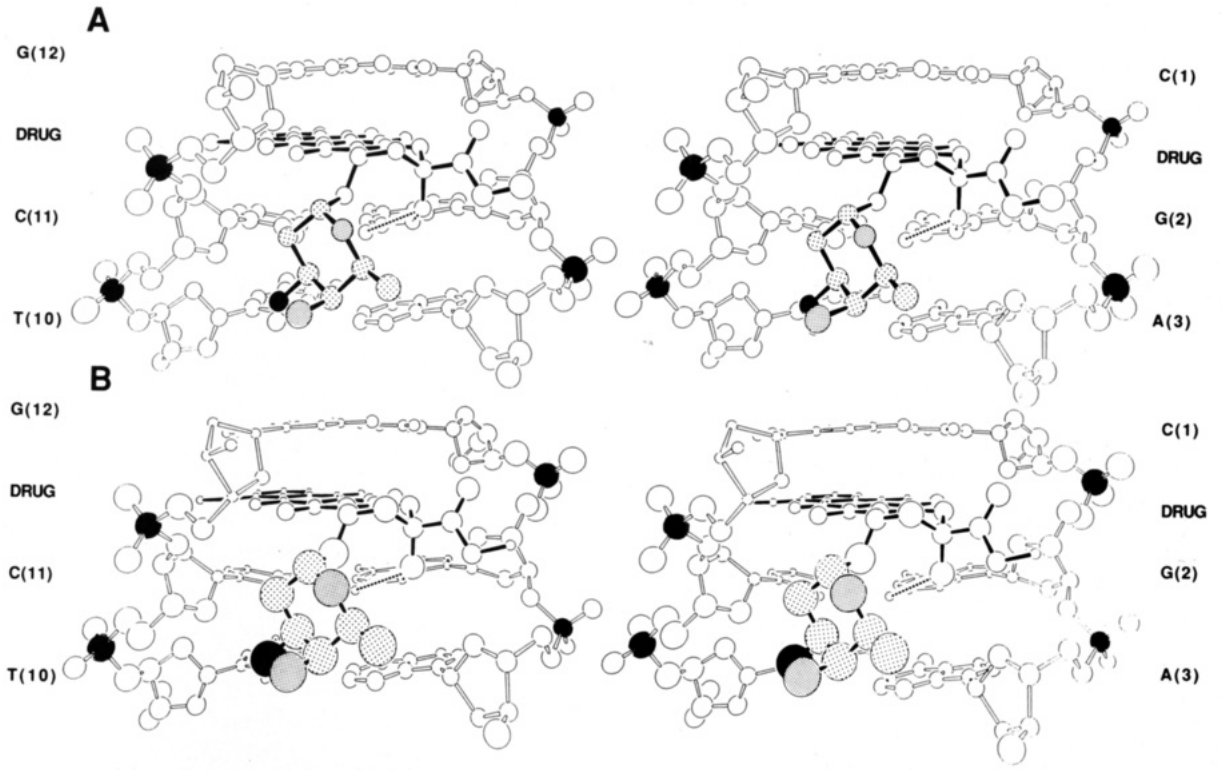

FIGURE 2: Stereo ORTEP representations of the LT-ADRI complex. In (A), the atoms are sized according to crystallographic displacement factors. In (B), the atoms are sized according to ΔB ($B_{RT} - B_{LT}$) factors. In both figures, the DNA is drawn with hollow bonds and the adriamycin with solid bonds. Atom types are coded by stippling, with the black nitrogen atom of the amino sugar darker than DNA phosphorus atoms, which are darker than oxygen atoms of the amino sugar, which are darker than carbon atoms of the amino sugar. All other atoms are white. Hydrogen-bonding interactions between D(15) O9 and G(2) N2 and N3 are drawn with dashed lines. In (A), atoms are scaled by 50% probability, and in (B), the atoms are scaled by 60% probability (determined by ΔB).

three for LT-ADRI ($1/2 - y$, $1/2 + x$, $1/4 + z$ and $3/2 - y$, $x - 1/2$, $1/4 + z$), d(GG^{Br}UA^{Br}UACC) ($1 - y$, $x - y$, $1/3 + z$ and $y - x + 1$, $1 - x$, $2/3 + z$), and d(CpG)–proflavine ($x - 1$, y, z and $x + 1$, y, $z - 1$). The total number of cyclic structures counted by CYCLONE was greater when three duplexes were used in the coordinate file, but the relative numbers of each type of n-membered ring were unchanged.

The numbers of n-membered rings found by CYCLONE were plotted versus M, where M represents the number of n-membered rings expected from random association of water molecules. The independent variable M is a function both of the number of water molecules in the box (w) and the number of unique rings formed by n water molecules. M was calculated as shown below.

$$M = [(w)!/2(w - n)!(n)]$$

In this equation, $n = 5$ for pentagons, $n = 4$ for tetragons, and $n = 3$ for triangles, etc.

RESULTS

The conformation and DNA–drug interactions of the d(CGATCG)–anthracycline complexes reported here (Figure 2) are very similar to the original room-temperature structures (Frederick et al., 1990). In both structures, the chromophore is intercalated at the d(CpG) steps on each end of the duplex, with the two amino sugars lying in the minor groove. The 9-hydroxyl oxygen of the drug chromophore is within hydrogen-bonding distance of both N2 and N3 of G(2), and the 3′-amino nitrogen of the amino sugar forms hydrogen bonds to T(10) O2, C(11) O2, and C(11) O4′. Superposition of the RT- and LT-d(CGATCG)–ADRI coordinates (data not shown) indicated that the two structures are very similar.

In comparison to the RT sum maps, the LT maps were of greater quality, displaying finer detail and allowing more confident placement of solvent molecules. The quality of the electron density maps is demonstrated in Figure 3A,B, where stereoviews of the LT-DAUN sum map in the vicinity of the backbone (Figure 3A) and A(3)-T(10) base pair (Figure 3B) are displayed. Our direct comparison of the LT- and RT-DAUN sum maps has revealed that the LT maps are of superior quality, presumably because of the increased number of reflections in the LT data sets. The high-quality sum maps provide the opportunity to address three important issues: (1) For n-membered water rings near nucleic acid surfaces, is $n = 5$ preferred over other n-membered rings? (2) What are ideal hydrogen-bond geometries, and how are these modulated by the interface with DNA? (3) What are the relative contributions of thermal and static disorder to displacement factors in crystals of these DNA–anthracycline complexes?

Cyclic Structures. We have constructed and employed a Fortran program, CYCLONE, that counts n-membered rings. This program was used to analyze the single-crystal X-ray structures of LT-ADRI, LT-DAUN, d(GG^{Br}UA^{Br}UACC) (Kennard et al., 1986), and d(CpG)–proflavine (Schneider et al., 1992). We hypothesized that, in the absence of greater stability of one n-membered water ring relative to other ring sizes, the probability of occurrence (Q) of each ring size should be linearly related to M. The variable M represents the number of possible unique n-membered rings formed by the water molecules in the box.

To understand the relationship between M and Q, CYCLONE was used to count numbers of n-membered rings formed by water molecules separated by 4.5–5.0 Å. Hydrogen bonding is not expected to influence the relative

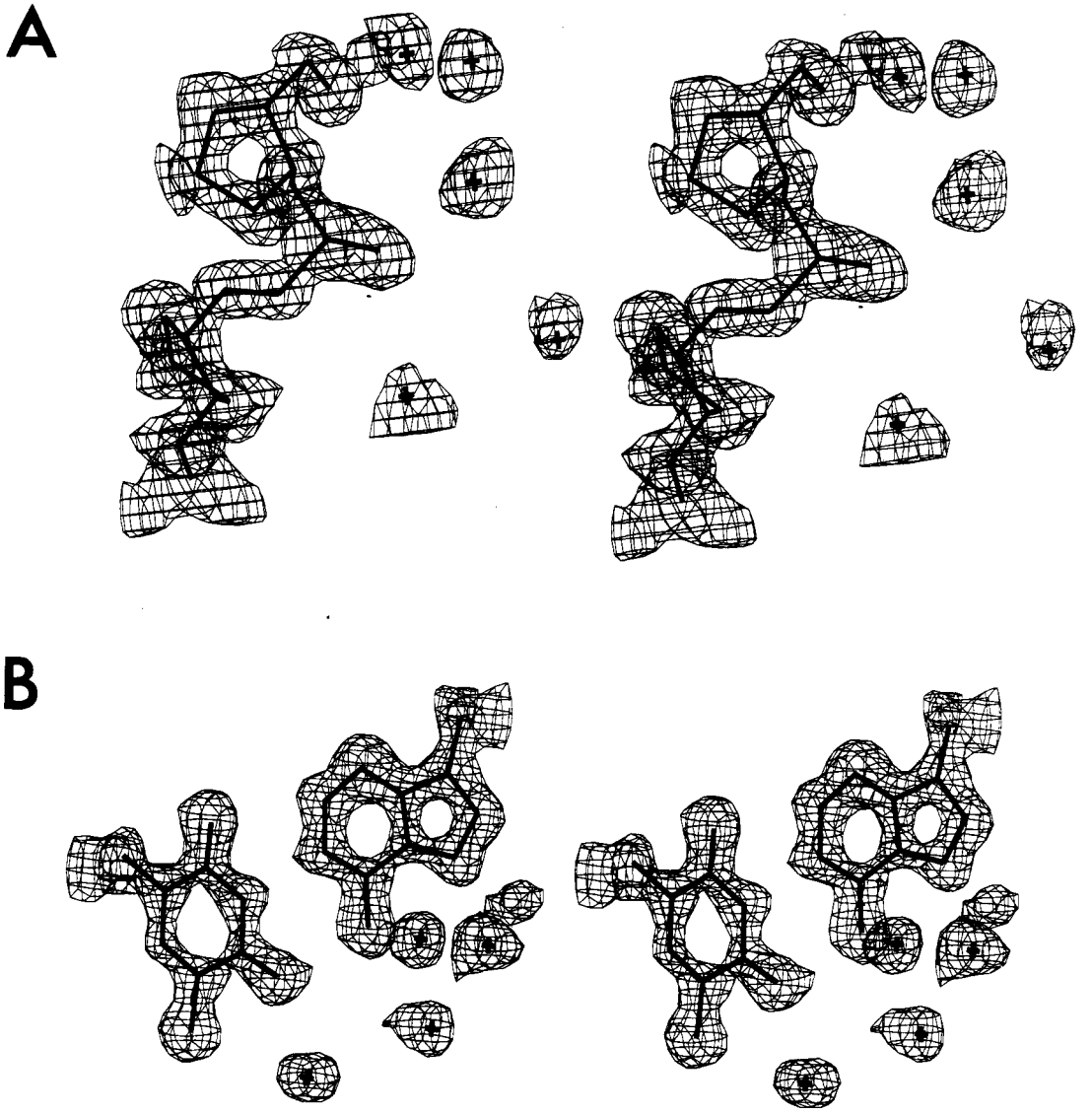

FIGURE 3: Sum map in the vicinity of (A) the deoxyribose-phosphate backbone and (B) the adenine-thymine base pair.

frequencies of ring sizes formed by water molecules separated by these distances. As discussed below, these water molecules are noninteracting. For n-membered rings composed exclusively of noninteracting water molecules, log Q is plotted versus log M for LT-ADRI (Figure 4), d(CpG)–proflavine (Figure 1S), and GG^{Br}UA^{Br}UACC (Figure 2S). In these cases, the relative numbers of ring types are predicted by the number of possible ways that each ring type can form. This observation validates the relationship between Q and M and indicates that five-membered rings are not preferred over other ring types for noninteracting water molecules.

Hydrogen-bonded water rings are composed of water molecules separated by less than 3.4 Å. As discussed below, these water molecules are interacting via hydrogen bonds. Numbers of n-membered hydrogen-bonded rings were counted with CYCLONE. For interacting water molecules, Figures 5, 3S, and 4S are log–log plots of Q versus M for LT-ADRI, d(GG^{Br}UA^{Br}UACC) (Kennard et al., 1986), and d(CpG)–proflavine (Schneider et al., 1992), respectively. Statistical analysis reveals that, in all three duplexes, the $n = 5$ point is not significantly (within 95% confidence limits) above the line.

Hydrogen-Bond Geometry. An important goal of this study was to characterize geometry of water–DNA and water–water hydrogen bonds. However, hydrogen atoms are not observed

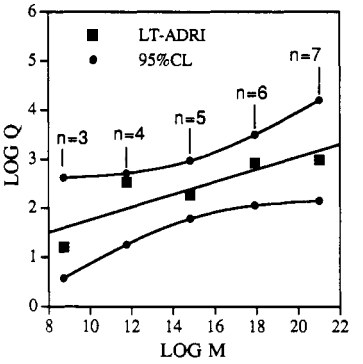

FIGURE 4: Plot of log Q versus log M, where Q equals the number of n-membered rings formed by water molecules separated by distances of 4.5–5.0 Å. M is a function of both the number of unique rings formed by n water molecules, $(n - 1)!/2$, and the number of water molecules in the box considered by CYCLONE (see Experimental Procedures for a discussion of this calculation). The equation of the best-fit line is log $Q = 0.47 + 0.13$ log M with $\chi^2 = 0.75$. The curved lines represent the upper and lower limits of the 95% confidence interval.

by X-ray data of the quality described here, and therefore, hydrogen bonds must be inferred from geometry. To characterize hydrogen-bonding geometry, it is necessary to establish an appropriate cutoff distance (between heteroatoms) beyond

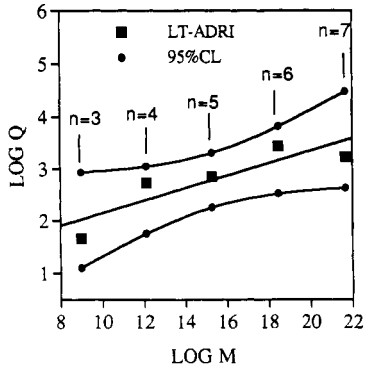

FIGURE 5: Plot of log Q versus log M for LT-ADRI, where Q equals the number of n-membered rings formed by water molecules separated by 3.4 Å or less. The equation of the best-fit line is log Q = 0.920 + 0.12 log M with χ^2 = 0.78. The curved lines represent the upper and lower limits of the 95% confidence interval.

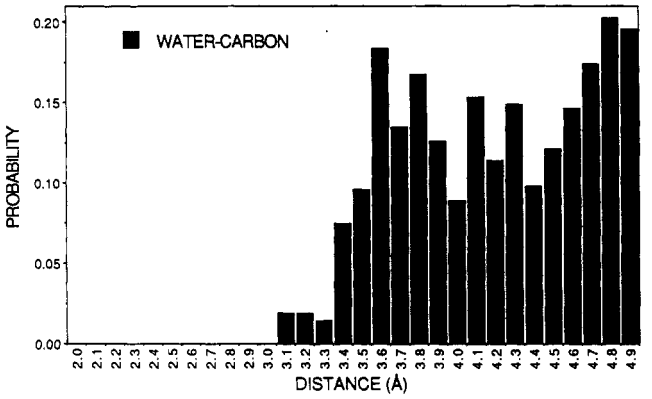

FIGURE 6: Histogram of water–carbon distances. The probability was obtained by taking the number of water–carbon distances within a 0.1-Å range (for example, between 3.0 and 3.1 Å) and dividing it by the total number of water–carbon contacts up to 5.0 Å.

which it can be reasonably concluded that a hydrogen bond does not link two atoms. The determination of such a cutoff distance is somewhat subjective, and previous investigations have used cutoff distances ranging from 3.25 Å (Berman et al., 1988) to 5.0 Å (Yanagi et al., 1991). To establish a reasonable hydrogen-bond cutoff distance, we gathered statistics on water–carbon interatomic separations (see Figure 6). The formation of CH···A (where A = acceptor) hydrogen bonds is not common, and the distribution of C–water distances should be very similar to the distribution of non-hydrogen-bonded water–water distances. The results show that water molecules are not found less than 3.1 Å from carbon atoms and only rarely within 3.4 Å (Figure 6). The frequency of occurrence rises abruptly when the interatomic separation reaches 3.4 Å. This indicates that 3.4 Å is a common, non-hydrogen-bonded interatomic distance when one of the atoms is a carbon. It is likely that the same is true when the atoms involved are either water oxygens or other DNA heteroatoms. Therefore, heteroatoms separated by 3.4 Å or less are considered here to be within hydrogen-bonding distance, and those separated by distances greater than 3.4 Å are considered to be noninteracting.

For the LT-ADRI and LT-DAUN structures, we have divided the water molecules into two classes based on their distances from the DNA. All water molecules within 3.4 Å of any DNA atom were classified as first (F) shell, while all others were included in the second (B) shell (where B denotes the similarity of this shell to bulk water). LT-ADRI contains 42 F waters and 20 B waters, while LT-DAUN contains 32 F waters and 23 B waters.

Table 2: Average Hydrogen-Bond Lengths (Å)[a]

	LT-ADRI	LT-DAUN
DNA–water[b]	2.86 (0.04)[c]	2.95 (0.05)
first-shell water–water[d]	2.77 (0.04)	2.85 (0.05)
second-shell water–water[e]	3.10 (0.07)	2.92 (0.09)
water–water (all)[f]	2.78 (0.03)	2.85 (0.04)

[a] This data was collected at −160 °C. All hydrogen-bond lengths given in this table refer to the distances between heteroatoms. For example, water–water hydrogen-bond lengths give the distance between the water oxygens. An example of a DNA–water hydrogen-bond length would be the distance between a guanine N2 and a water oxygen. [b] These are the average hydrogen-bond lengths for all DNA–water contacts shorter than 3.4 Å. Interactions of first-shell waters with the bases, phosphates, and deoxyriboses have been grouped together. [c] The number in parentheses represents the 95% confidence limit. [d] These are average lengths for water–water separation distances involving first-shell water molecules. It includes both water (F)–water (F) and water (F)–water (B), where F and B represent the primary (first) and secondary (bulk) hydration shells. [e] These are average lengths for water–water hydrogen bonds of the type water (B)–water (B). [f] These are average lengths for all water–water separation distances. Water (F)–water (F), water (F)–water (B), and water (B)–water (B) have been grouped together.

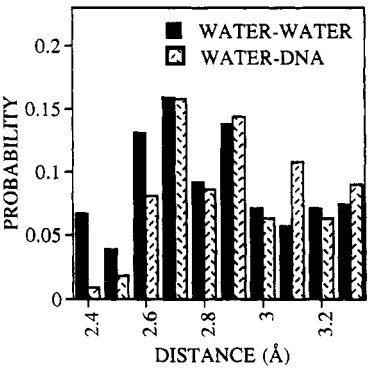

FIGURE 7: Histogram of water–water and water–DNA distances. It should be emphasized that these are heteroatom distances; the water–water distances are between water oxygens, and the water–DNA distances are between the water oxygen and the DNA nitrogens or the DNA oxygens. The water–DNA category includes both water–DNA and water–anthracycline distances. Water–nitrogen and water–oxygen distances have been grouped together. The probability was obtained by taking the number of distances within a 0.1-Å range (for example, between 3.0 and 3.1 Å) and dividing it by the total number of distances up to 5.0 Å. The water–water histogram is given in black, while those for water–DNA are stippled.

The length of the average water–DNA hydrogen bond is not significantly different from the length of the average water–water hydrogen bond. For both LT-ADRI and LT-DAUN, the average water–DNA hydrogen-bond lengths fall barely (0.01 Å) outside of the 95% confidence interval for water–water hydrogen-bond lengths. This difference is demonstrated in Table 2, where average hydrogen-bond lengths for LT-ADRI and LT-DAUN are listed with the 95% confidence levels in parentheses. Figure 7 shows the histogram of hydrogen-bond distances for LT-ADRI. As will be discussed below, the distribution of distances is very similar to that observed in the crystal structures of small biological molecules.

It appears that water molecules in contact with the DNA, on average, assume less favored hydrogen-bonding geometry than other water molecules. Although the averages of the first- and second-shell water–water–water angles are not statistically different from each other or from the water–DNA–water angles (Table 3), the second-shell water–water–water angles are more narrowly distributed than first-shell water–water–water angles. This difference is demonstrated in Figure 8, where a histogram of hydrogen-bond angles is shown. The majority of second-shell water–water–water

Table 3: Average Hydrogen-Bond Angles (degrees)[a]

	LT-ADRI	LT-DAUN
water–DNA–water	99.3 (3.9)[b]	105.2 (4.1)
first-shell water–water–water[c]	104.1 (6.3)	106.8 (6.0)
second-shell water–water–water[d]	105.9 (6.4)	97.9 (24.7)
overall water–water–water[e]	104.8 (4.6)	105.9 (5.9)

[a] These data were collected at −160 °C. Angles given in this table refer to angles between heteroatoms. For example, a water–water–water angle refers to the angle between three water oxygen atoms. [b] The number in parentheses represents the 95% confidence limit. [c] These are average water–water–water angles for the first shell. They include water (F)–water (F)–water (F), water (F)–water (F)–water (B), and water (F)–water (B)–water (B) systems, where F and B represent the primary (first) and secondary (bulk) hydration shells. [d] These are average angles for water (B)–water (B)–water (B) systems. [e] These are average angles for all water–water–water systems. The primary (F) and secondary (B) hydration shells have been grouped together.

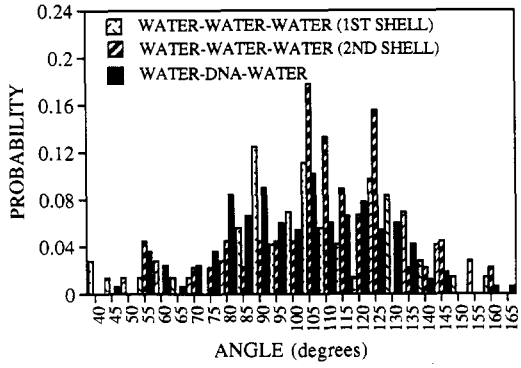

FIGURE 8: Histogram of first-shell water–water–water, second-shell water–water–water, and water–DNA–water angles. As was the case for Figure 7, the values given are between heteroatoms, and the water–DNA–water category includes both water–DNA–water and water–anthracycline–water angles. The probability was obtained by taking the number of angles within a 5° range (for example, between 95° and 100°) and dividing it by the total number of interactions. The distribution of water–DNA–water angles is shown in gray, while those for first-shell water–water–water and second-shell water–water–water are stippled.

angles assumes values between 105° and 125°, while the first-shell water–water–water or water–DNA–water angles are more broadly distributed between 90° and 130° (see Discussion).

The water–DNA category of Figure 7 includes both water–DNA and water–drug distances. A large percentage of these are water–oxygen interactions. For example, of 56 unique water–DNA hydrogen bonds for LT-ADRI, 39 (70%) involve hydrogen-bond-accepting oxygens of the base, deoxyribose, or phosphate backbone, 7 (12%) involve drug oxygens, and only 10 (18%) involve base or drug nitrogens. Because 70% of water–DNA hydrogen bonds involve water–oxygen interactions and because the oxygens of the base, deoxyribose, and phosphate backbone are exclusively hydrogen-bond acceptors, water acts as a donor in the majority of water–DNA hydrogen bonds. It seems reasonable to compare the water (donor)–oxygen (acceptor) hydrogen-bond length distributions of Jeffrey and Maluszynska (1990) with the water–DNA distributions reported here. With the exception of the terminal hydroxyl groups, DNA hydrogen-bond-donor sites are exclusively nitrogen atoms.

Mobility. The amino sugar is the most thermally mobile portion of the complex. At room temperature, both static disorder and thermal motion contribute to isotropic displacement factors (B). At −160 °C, thermal motion is negligible and static disorder provides the only significant contribution to displacement factors. By taking the difference between

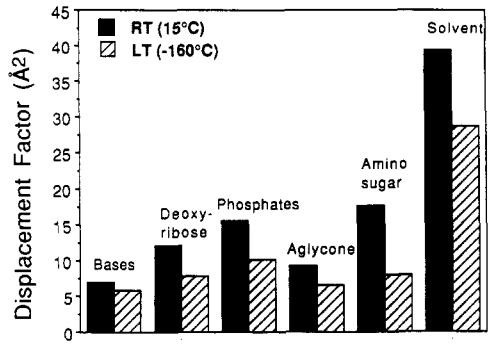

FIGURE 9: Bar graph of average RT and LT crystallographic displacement factors for the DNA base atoms, deoxyribose, phosphates, drug chromophore, drug amino sugar, and solvent molecules. The RT values are in black, while those for the LT values are stippled.

Table 4: Average Displacement Factors (Å²)[a]

	LT-ADRI	LT-DAUN
	DNA	
bases	5.97 (0.18)[b]	5.57 (0.21)
deoxyriboses	7.79 (0.23)	6.97 (0.26)
phosphates	10.04 (0.53)	10.02 (0.74)
	Anthracycline	
chromophore	6.78 (0.23)	5.49 (0.16)
amino sugar	7.76 (0.50)	6.38 (0.31)
	Water	
first shell (F)	24.57 (2.52)	20.86 (2.50)
second shell (B)	33.79 (4.48)	30.69 (3.66)
conserved[c]	24.05 (2.69)	20.44 (2.43)
overall (F and B)	27.31 (2.31)	25.07 (2.32)

[a] These data were collected at −160 °C. [b] The number in parentheses represents the 95% confidence limit, calculated as [(1.96)(standard deviation)/($\sqrt{N}$)], where N equals the number of observations. [c] These solvent atoms were observed in both the present LT work and the original RT structure (Frederick et al., 1990). LT-waters which were within 1.5 Å of RT-solvent atoms were included in this category. The value of 1.5 Å was chosen as the cutoff criterion because the correspondence became ambiguous beyond this distance. Thirty-one daunomycin water molecules (23 first shell and 8 second shell) and 29 adriamycin water molecules (21 first shell and 8 second shell) were found to meet this criterion.

the RT and LT displacement factors, thermal motion is isolated. The Δdisplacement factor (ΔB) for each atom is determined by $B_{RT} - B_{LT}$. Thus, ΔB gives a measure of molecular motion, unobscured by static disorder, within a crystal.

For each group of atoms, the LT (static only) and RT (static plus thermal) displacement factors are shown in a bar graph in Figure 9. LT displacement factors for ADRI–d(CGATCG) and DAUN–d(CGATCG) increase in the order: base < chromophore < deoxyribose, amino sugar < phosphates < conserved first- and second-shell waters, first-shell waters < second-shell waters (see Table 4). In contrast, the thermal mobility (given by ΔB) experienced by atoms in the crystal increases in the order: bases < chromophore < deoxyribose < phosphates < amino sugar, solvent. Thermal mobility is illustrated in Figure 2B where LT-ADRI atoms are scaled according to ΔB. The amino sugar displays the highest thermal mobility. In contrast, the phosphate groups display the greatest static disorder (Table 4). Thus, the phosphate positions vary from site to site within the crystal but do not change significantly with time, while the position of the amino sugar varies during the RT data collection process.

Ions. The assignment of ions to electron density peaks is problematic. Three cations were present in the crystallization medium, sodium, magnesium, and spermine. The criteria used to identify potential monocations are as follows: (1) an

unusually low displacement factor, (2) six contacts to other atoms, and (3) coordination geometry inconsistent with a stable hydrogen-bonding arrangement. A single "water" molecule in each structure satisfied these criteria to the extent that it is reasonable to conclude it is partially occupied by a monocation and partially by a water molecule. These "water" molecules are W(17) 12 in LT-DAUN and W(17) 05 in LT-ADRI. The displacement factor of each is relatively low [10.3 Å^2, W(17) 12, and 10.5 Å^2, W(17) 05], and there are a large number of contacts to other atoms [6 to W(17) 12 and 5 to W(17) 05]. Both W(17) 12 (LT-DAUN) and W(17) 05 (LT-ADRI) are in contact with G(6) N7, D(13) O4, D(13) O5, and two other water molecules. An additional contact to a third water molecule is formed by W(17) 12 of LT-DAUN.

The coordination lengths (~2.8 Å) and numbers (5–6) are hybrids of those expected for an ion and for a water molecule. It is likely that these two "water" molecules are actually partially occupied sodium or magnesium (with lower occupancy) ions. The equivalents of both W(17) 12 and W(17) 05 were refined as sodium ions in the RT structures (Frederick et al., 1990) but have been refined as water molecules here. Careful search of the LT sum and difference electron-density maps did not reveal evidence of spermine molecules. The spermine molecules observed at RT (Frederick et al., 1990) are not present in the LT structures, even though the crystallization conditions were quite similar.

Water molecules W(17) 01, W(17) 02, and W(17) 03 are well ordered in both LT-ADRI and LT-DAUN. All of these water molecules have displacement factors (both LT-ADRI and LT-DAUN) under 9 Å^2. These values are significantly lower than the average displacement factors for first-shell water molecules (see Table 4). The four-coordinate geometry of each indicates that W(17) 01, W(17) 02, and W(17) 03 (both LT-ADRI and LT-DAUN) are indeed water molecules. Each of these water molecules has four contacts to electronegative atoms, and the coordination lengths fall between 2.6 and 3.3 Å, a range characteristic of hydrogen bonds. In addition, the hydrogen-bond angles are close to those observed in tetrahedral arrangements (108°).

Data Quality. Two major differences in the means of data collection for the RT (Frederick et al., 1990) and LT (reported here) structures are the X-ray detectors (multiwire area detector for LT versus diffractometer for RT) and the temperature (15 versus −160 °C). It is unclear whether the area detector or the LT (or both) is responsible for the increased number of reflections being observed in the present structures. It is worth noting that the LT (−130 °C) crystallographic data set of d(CpG)–proflavine (Schneider et al., 1992) contained nearly twice as many unique reflections [$F > 2\sigma(F)$] as the −2 °C structure, even though both data sets were collected with a diffractometer.

DISCUSSION

Cyclic Structures. Water molecules embedded in five-membered rings have been described in a series of protein and DNA crystal structures. In the structure of insulin, the valine 3 side chain is caged by three fused five-membered water rings (Baker et al., 1985). Three of five edge-linked five-membered water rings on the surface of crambin (Teeter, 1984; Teeter & Whitlow, 1987) share a common apex which caps a leucine methyl group. The hydration of crambin (Teeter & Whitlow, 1987) is similar to that found in clathrates of ethylene oxide deuterohydrate and *n*-propylamine hydrate. In crambin, insulin, and clathrate crystal structures, five-membered water rings preferentially form around hydrophobic surfaces (Jeffrey & Saenger, 1991). Nucleic acid surfaces are hydrophilic and highly charged. Thus, one might not expect to observe five-membered rings at DNA interfaces.

However, there are numerous reports of five-membered rings near DNA surfaces. In the RT-d(CpG)–proflavine complex (Neidle et al., 1980), five edge-linked five-membered water rings are within hydrogen-bonding distance of guanine O6 and N7, cytosine N4, and a proflavine atom (N10). The formation of five-membered water rings in that structure was verified by recollection of X-ray intensity data at −2 °C (Berman & Ginell, 1986) and −130 °C (Schneider et al., 1992). In addition, a ribbon of five-membered rings interacts with the phosphate oxygens and bases of two isomorphous A-DNA octamers, d(GG^{Br}UA^{Br}UACC) and d(GGTATACC) (Kennard et al., 1986). In these A-DNA structures, water forms five-membered rings surrounding the thymine methyl groups of d(GGTATACC) and the bromine atoms of d(GG^{Br}UA^{Br}UACC). Finally, an isolated five-membered ring of water molecules has been observed hydrogen bonded to G(3) O6, G(3) N3, C(4) N4, and G(13) O6 in an A-conformation octamer of d(GTGCGCAC) (Bingman et al., 1992).

Our original intention was to measure populations of ring types to determine their relative free energies of formation. A common theme from previous studies is the lack of a systematic method for determining ring size frequencies. The difficulty of accurately counting a given ring size increases dramatically with *n*. We have devised a thorough and unbiased means of counting cyclic type frequencies with the program CYCLONE. As a control for determining the distribution of random ring sizes, we have determined frequencies of ring sizes for noninteracting water molecules (separated by 4.5–5.0 Å). We have compared the noninteracting and interacting frequency distributions. Interacting cycles contain water molecules separated by no more than 3.4 Å. This analysis has been performed on LT-ADRI (Figure 5), LT-DAUN (data not shown), d(CpG)–proflavine (Figure 3S) (Schneider et al., 1992), and d(GG^{Br}UA^{Br}UACC) (Figure 4S) (Kennard et al., 1986). The results show that five-membered rings are not preferably formed by water molecules near DNA and DNA–drug complexes. The unambiguous conclusion is that five-membered water rings are not overrepresented near nucleic acid surfaces.

In some cases, the cooperative nature of hydrogen bonding may lead to stabilization of rings over random patterns of association (Jeffrey & Saenger, 1991). Hydrogen bonds polarize water molecules. Rings maximize the induced polarities. Within the limits of geometric restaints, the smaller the ring, the greater the polarization and the greater the cooperativity. Rings with four, five, and six members should be of greatest stability. Near a hydrogen-bonding surface, cooperatively stabilized rings require surface-bound hydroxyl groups acting simultaneously as donors and acceptors. A network of rings has been reported in crystal structures of hydrated α-cyclodextrin, whose surface is well covered with hydroxyl groups (Saenger et al., 1985). In this case, rings with four, five, and six members are overrepresented relative to rings with three or seven members. By this analysis, cooperative rings would be uncommon near DNA. DNA contains an imbalance of hydrogen-bond donors and acceptors and lacks hydroxyl groups. It is reasonable to suggest that the number of cooperative rings in the structures of LT-ADRI, CpG–proflavine, and GG^{Br}UA^{Br}UACC is small in comparison to the number of noncooperative cycles (which have no energetic advantage). If so, rings with $n = 4$, 5, and 6 should

not be overrepresented, consistent with the observations reported here.

Hydrogen-Bond Geometry. High-resolution, small-molecule crystallography has revealed that a hydrogen bond in which a water molecule acts as a donor and an oxygen in a biological molecule acts as an acceptor is slightly longer and more tightly restrained than a water–water hydrogen bond (Jeffrey & Maluszynska, 1990). Although we do not observe hydrogen atoms in large-molecule crystallography, it is possible to make many hydrogen-bond-donor/-acceptor assignments based on the known tautomeric states of DNA. As noted by Quigley (1987), in DNA there are many more hydrogen-bond-acceptor than -donor sites. Further, the acceptor sites are predominantly oxygen atoms. Although the water–nitrogen and water–oxygen distances have been grouped together in Figure 7, the vast majority of these are water (donor)–oxygen (acceptor) interactions. The distribution of distances observed in Figure 7 is remarkably similar to that expected from crystal structures of small biological molecules in which water is a donor and oxygen is an acceptor.

This similarity promotes confidence in the quality of the data and location of the LT-ADRI and LT-DAUN water molecules and suggests that hydration patterns in small-molecule crystal structures are consistent with hydrogen-bonding geometry in macromolecules.

If any particular ring size were preferred, one would expect a narrow distribution of first-shell water–water–water angles. We have characterized the water–DNA–water, first-shell water–water–water, and second-shell water–water–water hydrogen-bond angles in LT-ADRI. The results demonstrate (see Figure 8) that hydrogen-bond angles are widely distributed near the DNA surface, consistent with our conclusion that the water structure around these DNA–anthracycline complexes does not prefer five-membered rings.

First-shell water molecules assume less favored configurations than second-shell water molecules. The distribution of water–DNA–water hydrogen-bond angles (see Figure 8) differs from that of first-shell water–water–water and second-shell water–water–water hydrogen-bond angles. The second-shell water molecules, which are not forming hydrogen bonds to the DNA, have water–water–water angles more narrowly distributed than either the first-shell water–water–water or water–DNA–water angles. For example, there is approximately a 60% probability of second-shell water–water–water angles occurring in a narrow 20° range (105°–125°) and first-shell water–water–water and water–DNA–water angles occurring in a 40° range (either 80°–120° or 90°–130°). These results are consistent with those from hydrogen-bond energy calculations (Hagler et al., 1974) that suggest that angle deviations as large as 20° do not significantly affect the energy of interaction. The second-shell water–water–water angles are narrowly distributed around those observed in ice (Jorgensen & Worlton, 1985; Kamb et al., 1967). In addition, water–DNA–water angles have an approximately Gaussian frequency distribution which reaches a maximum at 105°. In contrast, the distribution of first- or second-shell water–water–water angles is not nearly so symmetrical. While differences are observed in the hydrogen-bond angle distributions, the average first- and second-shell water–water–water angles are not statistically different from those of water–DNA–water. These values are given for both LT-ADRI and LT-DAUN in Table 3.

Mobility. Our calculation of ΔB factors suggests that the anthracycline amino sugar experiences considerable thermal motion in the crystal. This result is consistent with those from X-ray crystal structure determinations of anthracyclines complexed to DNA of different sequences (Frederick et al., 1990; Leonard et al., 1992; Moore et al., 1989; Nunn et al., 1991; Quigley et al., 1980; Wang et al., 1987; Williams et al., 1990a,b). The position and interactions of the amino sugar were found to vary throughout the series of structures. In DAUN–d(CGTACG), DAUN–d(TGTACA), and 4′-*epi*-ADRI–d(TGTACA), the only hydrogen-bonding interactions of the amino sugar with the DNA are via solvent molecules. However, in ADRI–d(CGATCG), DAUN–d(CGATCG), and DAUN–d(TGATCA), the amino sugar is shifted significantly toward the floor of the minor groove, placing the N3′ within direct hydrogen-bonding distance of T(10) O2, C(11) O2, and C(11) O4′. A radically different position of the amino sugar is observed in the crystal structure of 11-deoxyDAUN–d(CGTsACG). In this case, the positively charged N3′ of the sugar forms both direct (with A(4) O4′ and T(3) O2) and solvent-mediated hydrogen bonds with the DNA. These structure determinations, together with the inability of minor-groove footprinting agents to detect daunomycin bound to DNA (van Dyke et al., 1982) and the ΔB values reported here, highlight the inherent mobility of the anthracycline amino sugar. Apparently, the amino sugar position observed in each crystal structure represents the lowest energy conformation within a fairly flat potential well.

This conclusion that the amino sugar is highly mobile may bear on the reliability of calculations of the sequence specificity of DNA–anthracycline interactions. Pullman (1989), using molecular electrostatic potentials, has calculated most favorable energies of interaction for the daunomycin amino sugar with hexamers containing the central base sequence d(AT). If d(CG) is substituted for the central d(AT), the interaction is thought to become less favorable due to repulsion between the sugar and the guanine 2-amino group. However, for a mobile amino sugar, there should be a low energy cost in avoiding the guanine amino group, and the energy difference (for the sugar-binding preference) between d(TATATA) and d(TACGTA) could be considerably less than the predicted value of around 20 kcal/mol.

The thermal mobility of each base pair appears to be dictated in part by the number of hydrogen bonds between that base pair and anthracycline. In a manner that is absent in normal B-DNA, the anthracycline acts as a conduit for hydrogen-bonding interactions to effectively transmit force along the helical axis. The ΔB factor was determined for each base pair by averaging over the atoms of that base pair (phosphate and deoxyribose excluded). The average ΔB factors are 1.04 (0.26) Å^2 for the terminal base pairs, 0.50 (0.12) Å^2 for the intermediate base pairs, and 2.08 (0.28) Å^2 for the central base pairs. The intermediate base pair, having the lowest ΔB factor, forms the greatest number of hydrogen bonds to the anthracycline. This base pair appears to be held fixed by direct hydrogen bonds from the 9-hydroxyl of the chromophore to N3 and N2 of G(2) and from the 3′-amino group of the amino sugar to C(11) O2. The innermost base pair, with greater mobility than the intermediate base pair, is held by only a single hydrogen bond, from T(10) O2 to D(16) N3′. This base pair interacts with a relatively mobile portion of the anthracycline.

The terminal base pair, however, with no hydrogen bonds to the anthracycline, displays intermediate mobility. This result is in contrast with the observation of high mobility of the terminal base pairs in NMR studies of d(CGTACG)–morpholinylanthracycline complexes in solution (Odefey et al., 1992) but consistent with those from another crystallo-

graphic approach. In the anisotropic refinement of room-temperature X-ray diffraction data for DAUN–d(CGTACG), Holbrook (1988) observed that the average displacement factor (static plus thermal disorder) of the terminal base pairs is lower than that of the innermost base pairs.

Differences in the terminal base pair mobility observed in NMR and crystallography likely arise from lattice effects. Perhaps stacking interactions between adjacent duplexes in the crystal hold the terminal bases more fixed than in solution.

Holbrook (1988) observed similar anisotropic displacement factors for the terminal and intermediate base pairs. In contrast, the Δdisplacement factors for the terminal and intermediate base pairs are significantly different. The Δdisplacement factors provide an accurate assessment of molecular mobility. The thermal motion contribution to RT displacement factors is obscured by the contribution from static disorder.

Missing Spermine Molecules. The absence of bound spermine molecules in LT-ADRI and LT-DAUN indicates that in DNA–anthracycline complexes, the DNA sequence d(CGATCG) is not a sufficient condition for the observation of crystallographically ordered spermine. Williams and co-workers (1990b) previously suggested a sequence dependence for spermine binding to DNA–anthracycline complexes. They compared the spermine interactions of RT-DAUN [d(CGATCG)] (Frederick et al., 1990), RT-ADRI [(d(CGATCG)] (Frederick et al., 1990), and d(CGATCG)–4′-*epi*ADRI. The observation was that each spermine is in a different orientation within a continuous hydrophobic zone formed by the 5-methyl and C6 of a thymine, C5 and C6 of a cytosine, and the drug chromophore. It was proposed that differences in spermine binding are dictated by modifications of the anthracyclines. The lack of ordered spermine in the d(CGTACG)–DAUN structure (Wang et al., 1987) strongly suggested a sequence dependence for spermine binding to DNA–anthracycline complexes. The continuous hydrophobic zone, which can only be formed by the sequence d(CGATCG), was thought to be a prerequisite for the observation of crystallographically ordered spermine.

However, the results here demonstrate that the DNA sequence d(CGATCG) is not a sufficient condition for the observation of crystallographically ordered spermine. The absence of spermine in LT-DAUN and LT-ADRI indicates that factors other than DNA sequence influence spermine binding to DNA–anthracycline complexes. These factors no doubt similarly influence specific spermine–DNA interactions, undermining the previous proposal that anthracycline modifications alone modulate these interactions.

Relevance to Solution Studies. In X-ray crystallographic studies of $[d(CGCGAATTCGCG)]_2$, Drew and Dickerson (1981) observed that the minor groove contains an ordered zig–zag array of water molecules (the spine of hydration). Recently, NMR studies of this same dodecamer in solution (Liepinsh et al., 1992) have shown that water hydrating the minor groove of DNA is characterized by residence times longer than 1 ns. Such long residence times were said to emphasize the important role of these water molecules in stabilizing the molecular structure of B-DNA. The hydration water molecules were detected by nuclear Overhauser effects with the adenine 2H protons (residues 5 and 6) and are thought to be part of the spine of hydration observed in the X-ray crystal structure.

Certain solvent molecules appear to be tightly bound to DNA–anthracycline complexes. Our criteria for tight binding are (1) relatively low displacement factor, (2) favorable geometry of interaction, (3) similar interaction with the DNA–drug complex in a variety of crystallographic environments, and (4) full occupancy by a single species. In both LT-ADRI and LT-DAUN, water molecule W(17) 01 has a relatively low displacement factor and forms good hydrogen bonds to T(4) O2, T(10) O2, and the 3′-amino group of the amino sugar. A corresponding water molecule is found in the complex of 11-deoxyDAUN–d(CGTsACG), in a different crystal form with different crystal-packing interactions. In a second example, in both LT-ADRI and LT-DAUN, water molecule W(17) 02 forms hydrogen bonds to C(7) O2 and O3 of the chromophore. A corresponding water molecule is found in the complex of 11-deoxyDAUN–d(CGTsACG). Water molecule W(17) 03, also with a low displacement factor, forms hydrogen bonds to the 2-amino group of G(6) in both LT-ADRI and LT-DAUN. Similarly, a corresponding water molecule is found in the complex of 11-deoxyDAUN–d(CGTsACG). Finally, both W(17) 05 (LT-ADRI) and W(17) 12 (LT-DAUN) interact with the N7 of G(6) and the O4 and O5 position of the chromophore and satisfy the criteria for tightly bound water molecules. However, as described above, these solvent molecules are likely to be partially occupied ions, and it is not correct to consider them as tightly bound water molecules. It is possible that the solvent molecules described here could be observed by newly developing NMR techniques.

ACKNOWLEDGMENT

The authors thank Drs. Martha Briggs and G. A. Jeffrey for helpful comments. We are also grateful to Dr. Helen Berman for providing reprints prior to publication and to Dr. Olga Kennard for coordinates of d(GG^{Br}UA^{Br}UACC).

SUPPLEMENTARY MATERIAL AVAILABLE

Plots of log Q versus log M for CpG–proflavin and GG^{Br}UA^{Br}UACC (5 pages). Ordering information is given on any current masthead page.

REFERENCES

Acramone, F., & Penco, S. (1989) in *Antitumor Natural Products* (Takeuchi, T., Nitta, K., & Tanaka, N., Eds.) pp 1–53, Japan Scientific Press, Tokyo.

Baker, T., Dodson, E., Dodson, G., Hodgkin, D., & Hubbard, R. (1985) in *Crystallography in Molecular Biology* (Moras, D., Drenth, J., Strandberg, B., Suc, D., & Wilson, K., Eds.) pp 179–192, Plenum Press, New York.

Berman, H. (1991) *Curr. Opin. Struct. Biol. 1*, 423–427.

Berman, H. M., Sowri, A., Ginell, S., & Beveridge, D. (1988) *J. Biomol. Struct. Dyn. 5*, 1101–1110.

Bingman, C., Li, X., Zon, G., & Sundaralingam, M. (1992) *Biochemistry 31*, 12803–12812.

Brunger, A., Kuriyan, J., & Karplus, M. (1987) *Science 235*, 458–460.

Chaires, J. B., Priebe, W., Graves, D. E., & Burke, T. G. (1993) *J. Am. Chem. Soc. 115*, 5360–5362.

Drew, H. R., & Dickerson, R. E. (1981) *J. Mol. Biol. 151*, 535–556.

Frederick, C. A., Williams, L. D., Ughetto, G., van der Marel, G. A., van Boom, J. H., Rich, A., & Wang, A. H.-J. (1990) *Biochemistry 29*, 2538–2549.

Gao, Y.-G., & Wang, A. H.-J. (1991) *Anti-Cancer Drug Des. 6*, 137–149.

Hagler, A. T., Lifson, S., & Huller, E. (1974) in *Peptides, Polypeptides and Proteins* (Blout, E. R., Bovey, F. A., Goodman, M., & Lotan, N., Eds.) pp 35–48, Wiley-Interscience, New York.

Hendrickson, W. A., & Konnert, J. H. (1981) in *Biomolecular Structure, Conformation, Function and Evolution* (Srinivasan, R., Ed.) Vol. 1, pp 43–57, Pergamon Press, Oxford.
Holbrook, S. R., Wang, A. H.-J., Rich, A., & Kim, S.-H. (1988) *J. Mol. Biol. 199*, 349–357.
Jeffrey, G. A. (1969) *Acc. Chem. Res. 2*, 344–352.
Jeffrey, G. A., & McMullan, R. K. (1967) *Progress Inorg. Chem. 8*, 43–108.
Jeffrey, G. A., & Maluszynska, H. (1990) *Acta Crystallogr. B46*, 546–549.
Jeffrey, G. A., & Saenger, W. (1991) in *Hydrogen Bonding in Biological Structures*, Springer-Verlag, New York.
Jorgensen, J. D., & Worlton, T. G. (1985) *J. Chem. Phys. 83*, 329–333.
Kamb, B., Prakash, A., & Knobler, C. (1967) *Acta Crystallogr. 22*, 706–715.
Kennard, O., Cruse, W. B. T., Nachman, J., Prange, T., Shakked, Z., & Rabinovich, D. (1986) *J. Biomol. Struct. Dyn. 3*, 623–647.
Kim, H. S., & Jeffrey, G. A. (1970) *J. Chem. Phys. 53*, 3610–3615.
Leonard, G. A., Brown, T., & Hunter, W. N. (1992) *Eur. J. Biochem. 204*, 69–74.
Liepinsh, E., Otting, G., & Wuthrich, K. (1992) *Nucleic Acids Res. 20*, 6549–6553.
Moore, M. H., Hunter, W. N., Langlois d'Estaintot, B., & Kennard, O. (1989) *J. Mol. Biol. 206*, 693–705.
Neidle, S., Berman, H., & Shieh, H. S. (1980) *Nature 288*, 129–133.
Nunn, C. M., Meervelt, L. V., Zhang, S., Moore, M. H., & Kennard, O. (1991) *J. Mol. Biol. 222*, 167–177.
Odefey, C., Westendorf, J., Dieckmann, T., & Oschkinat, H. (1992) *Chem.-Biol. Interact. 85*, 117–126.
Pullman, P. (1989) in *Advances in Drug Research* (Testa, B., Ed.) Vol. 18, pp 1–113, Academic Press, Boston.
Quigley, G. J. (1987) in *Transactions of the ACA* (Griffin, J. F., Ed.) Vol. 22, pp 121–130, Polycrystal Book Service, Buffalo.
Quigley, G. J., Teeter, M. M., & Rich, A. (1978) *Proc. Natl. Acad. Sci. U.S.A. 75*, 64–68.
Quigley, G. J., Wang, A. H.-J., Ughetto, G., van der Marel, G. A., van Boom, J. H., & Rich, A. (1980) *Proc. Natl. Acad. Sci. U.S.A. 77*, 7204–7208.
Sack, J. (1990) *Chain: A Crystallographic Modelling Program*, Baylor College of Medicine, Waco, TX.
Saenger, W., Betzel, Ch., Zabel, V., Brown, G. M., Hingerty, B. E., Lesyng, B., & Mason, S. A. (1985) *Proc. Int. Symp. Biomol. Struc. Interact., Suppl. J. Biosci. 8*, 437–450.
Schneider, B., Ginell, S. L., & Berman, H. M. (1992) *Biophys. J. 63*, 1572–1578.
Teeter, M. (1984) *Proc. Natl. Acad. Sci. U.S.A. 81*, 6014–6018.
Teeter, M., & Whitlow, M. D. (1987) in *Transactions of the ACA* (Griffin, J. F., Ed.) Vol. 22, pp 75–88, Polycrystal Book Service, Buffalo.
Trail, A., Willner, D., Lasch, S. J., Henderson, A. J., Hofstead, S., Casazza, A. M., Firestone, R. A., Hellstrom, I., & Hellstrom, K. E. (1993) *Science 261*, 212–215.
van Dyke, M. W., Hertzberg, R. P., & Dervan, P. B. (1982) *Proc. Natl. Acad. Sci. U.S.A. 79*, 5470–5474.
Wang, A. H.-J., Ughetto, G., Quigley, G. J., & Rich, A. (1987) *Biochemistry 26*, 1162–1163.
Williams, L. D., Egli, M., Ughetto, G., van der Marel, G. A., van Boom, J. H., Quigley, G. J., Wang, A. H.-J., Rich, A., & Frederick, C. A. (1990a) *J. Mol. Biol. 215*, 313–320.
Williams, L. D., Frederick, C. A., Ughetto, G., & Rich, A. (1990b) *Nucleic Acids Res. 18*, 5533–5541.
Xuong, N. H., Nielsen, C., Hamlin, R., & Anderson, D. (1985) *J. Appl. Crystallogr. 18*, 342–350.
Yanagi, K., Prive, G. G., & Dickerson, R. E. (1991) *J. Mol. Biol. 217*, 201–214.